

# Oxygen Interstitials in Superconducting $\text{La}_2\text{CuO}_4$ : Their Valence State and Role<sup>†</sup>

Kee Hag Lee<sup>\*,‡</sup> and Roald Hoffmann<sup>\*,§</sup>

Department of Chemistry and Research Institute of Basic Science, Wonkwang University, Iksan 570-749, Korea, and Department of Chemistry and Chemical Biology, Cornell University, Baker Laboratory, Ithaca, New York 14853

Received: June 11, 2005; In Final Form: July 28, 2005

The nature of the much debated valence state of an interstitial oxygen atom in oxygen-doped  $\text{La}_2\text{CuO}_4$  is the subject of this paper. In model cluster calculations, we studied the position, charge, and spin state of the interstitial oxygen atoms in this superconductor. The models considered allow the interstitial oxygen to move off a symmetrical position, to have varying spin and charge, and to be surrounded by various magnetic environments. UB3LYP calculations show that a model having an interstitial oxygen atom with a total spin of 1 is lowest in energy; the interstitial oxygen atoms here act as stable radicals with a net charge of  $-1$ . These results agree with experimental evidence for the paramagnetic behavior for interstitial atoms. The energy associated with a spin flip at a Cu site in our models is lower if interstitial oxygen has a local electron spin density, compared to the case when it does not. We provide a possible explanation for the increase of the doping concentrations of interstitial oxygen with a decrease of the Néel temperature of this system. The relative stability of the models we consider depends on their spin states, accompanied by structural changes; this explains indirectly the experimental change of the slope (from 2 to 1.3) of the linear relationship between the hole concentration and the oxygen content. Our results support a stripe phase in high temperature superconductivity; in our calculations, hole doping to the copper oxide layer comes only through the formation of an oxygen interstitial pair, not from any change of the local structural environment and magnetic field around the single interstitial.

Two decades of intense work after the breakthrough in high critical temperature ( $T_c$ ) superconductivity following Bednorz and Müller's discovery,<sup>1</sup> all really high  $T_c$  ceramic superconductors remain based on structures with square-planar copper oxide layers. These layers are then sandwiched between layers of other atoms, such as yttrium, barium, strontium, and lanthanum.

Each of the oxygen atoms in the copper oxide sheets, considered as  $\text{O}^{2-}$ , bears (formally) eight electrons. The Cu(II) atoms, in contrast, have an odd number of electrons and thus an excess electron spin, resulting in a net magnetism. In these materials, the spins are correlated; when one electron's spin points up, its neighbor prefers to point down. The copper spins align into three-dimensional antiferromagnetic long-range order at low temperatures. This large-scale pattern of behavior tends to prevent the free movement of charges, which enter the picture when these cuprate materials are doped with other atoms.

Both self-consistent field (SCF)<sup>2a,b</sup> and tight-binding band calculations<sup>2c</sup> indicate that the  $x^2-y^2$  band of tetragonal  $\text{La}_2\text{CuO}_4$  is half-filled and demonstrate that the charge density at the Fermi level consists mainly of interacting Cu  $d_{x^2-y^2}$  and oxygen p orbitals confined within the Cu–O layer.

One of the most striking features of the copper oxide superconductors is that they are all derived from charge-doped antiferromagnetic insulators. The parent compounds are insulating, due to correlations among localized electrons. Thus, using standard one-electron band theory to describe these materials leads to their characterization as nonmagnetic metals, which is clearly not correct. Better models have been proposed for the

electronic structure, and these describe properly the magnetism of the materials.<sup>2d</sup>

## What Happens upon Oxygen Doping: Experiment

The correct physical description of doped superconductors, however, is much more complicated.  $\text{La}_2\text{CuO}_4$  is the best-known cuprate, having the  $\text{K}_2\text{NiF}_4$  structure. The stoichiometric compound is an antiferromagnetic insulator but can be doped to produce a superconductor, with a maximum  $T_c$  as high as 40 K. Upon charge doping, typically of around 0.05–0.25 holes per  $\text{CuO}_2$ , the lamellar copper oxide materials become superconducting with short-range magnetic order.

Common doping methods include partially substituting La with alkaline earth metals (Ba, Sr)<sup>1</sup> or inserting interstitial oxygen into the structure.<sup>3</sup> The rare earth ions normally donate electrons to the electron-deficient atoms in the adjacent copper oxide planes. Since strontium has one less electron than lanthanum to donate, copper atoms wind up with electron vacancies, or "holes". These holes can percolate through the material, carrying a positive charge but no spin.

While Sr dopants are in fixed positions at the sample melting temperature near 1400 K, the excess oxygen dopants appear to be able to move. They eventually freeze into their equilibrium positions near 200 K, well below the relevant magnetic and electronic energies; the latter may be gauged by the antiferromagnetic exchange coupling between nearest neighbor Cu spins  $J \approx 1500$  K and the electronic bandwidth  $W \approx 2J$ . It was determined that the interstitial oxygen atoms occupy the sites between adjacent LaO layers.<sup>3</sup>

The anion-doped  $\text{La}_2\text{CuO}_{4+\delta}$  exhibits far more interesting physical properties than its cation-substituted counterpart. For example, there is the well-studied phase separation phenomenon in which the doped holes and interstitial oxygen atoms tend to form domains of different densities at about 320 K.<sup>3,4</sup> Jorgensen and co-workers<sup>4</sup> have carried out extensive studies on  $\text{La}_2$

<sup>†</sup> Part of the special issue "Donald G. Truhlar Festschrift".

<sup>\*</sup> To whom correspondence should be addressed. E-mail: rh34@cornell.edu (R.H.); khlee@wonkwang.ac.kr (K.H.L.).

<sup>‡</sup> Wonkwang University.

<sup>§</sup> Cornell University.

$\text{CuO}_{4+\delta}$ , concluding that the superconducting compound resulted from phase separation near room temperature into two quasi-isostructural orthorhombic phases. Additionally, the excess oxygen atoms were found to be located between the two LaO layers, surrounded by distorted cubes built up of two interpenetrated tetrahedrons, comprised of four La atoms and four oxygen atoms (from the apical oxygen atoms of the  $\text{CuO}_6$  octahedra), respectively.<sup>5,6</sup> In hole-rich domains, the hole exhibits a certain degree of ordering (also known as a stripe phase); this is regarded by some as a promising clue for understanding high temperature superconductivity.<sup>3,7,8</sup>

Chaillout and co-workers<sup>5</sup> interpreted the crystal structure of superconducting ( $T_c = 37.5$  K)  $\text{La}_2\text{CuO}_{4.032}$  (refined from single-crystal neutron diffraction data at room temperature and 15 K) by introducing oxygen occupancy factors in several models, involving either short or normal bonds. A discrete oxygen at the defect would exist as a charged species; then, it would contribute holes to the Cu–O sheets. A bonded species, very likely as peroxide, would require unexpected electron doping. This leaves open the question of the nature of the defect and how the system is doped.

Schirber and co-workers at Sandia National Laboratories (SNL)<sup>9</sup> suggest that the excess oxygen is incorporated in the structure as a superoxide  $\text{O}_2^-$  ion but is not present as  $\text{O}^{2-}$  or  $\text{O}_2^{2-}$ . This was determined by using a combination of electron microprobe microanalysis, iodometric titration, and weight gain measurements coupled with magnetization data and ion-size consideration. By using X-ray photoelectron spectroscopic (XPS) and annealing studies in the oxygen-enriched  $\text{La}_2\text{CuO}_{4+\delta}$ , Rogers and co-workers at SNL<sup>10</sup> reported the identification of superoxide as the predominant oxygen species correlated with a superconducting transition at 30 K. They cannot exclude a minority concentration of  $\text{O}^-$  by their XPS data.

Zhou and co-workers<sup>11</sup> reported that the superoxide resides on the surface, not in the bulk, and is not responsible for oxidizing the sample to the superconductive state. They also reported a first-order phase change from the superconductive state to the antiferromagnetic state with the loss of oxygen near 250 °C. This observation is suggestive of at least some suppression of the copper atomic moment in the superconductive phase. Shinn and co-workers at SNL<sup>12</sup> replied to a question of Strongin and co-workers,<sup>13</sup> who argued that the XPS evidence for superoxide<sup>10</sup> in  $\text{La}_2\text{CuO}_{4+\delta}$  was not sufficient, by arguing that the samples studied differ significantly. They further responded that the oxygen valences observed from XPS data (coupled with the paramagnetism in the superconducting  $\text{La}_2\text{CuO}_{4+\delta}$ ) suggest superoxide species, comprising a large fraction of the excess oxygen.<sup>12</sup>

Li and co-workers<sup>14</sup> studied a quantitative correlation of the excess oxygen content and corresponding hole concentration in  $\text{La}_2\text{CuO}_{4+\delta}$  for  $0 < \delta < 0.12$ . This was done in order to clarify important issues such as the valence state of the interstitial oxygen atoms, the excess oxygen content ( $\delta$ ), and the corresponding hole concentration. They observed two distinct sites, with a doping efficiency of 2 or 1.3 holes per excess oxygen atom. A critical carrier concentration ( $\delta \approx 0.06$ ) determined the occupation of the two different sites at room temperature. The parent compound, lanthanum cuprate ( $\text{La}_2\text{CuO}_4$ ), was reported to be an insulator with a band gap of about 2.0 eV.

Several groups have suggested that the predominant defect species are doubly charged oxygen interstitials, based on high temperature electrical conductivity and Seebeck coefficient measurements.<sup>15–17</sup>

Cordero and co-workers<sup>18</sup> reported that excess O in  $\text{La}_2\text{CuO}_{4+\delta}$  already starts forming two different types of defects at very low concentrations, as shown in anelastic spectra. The first

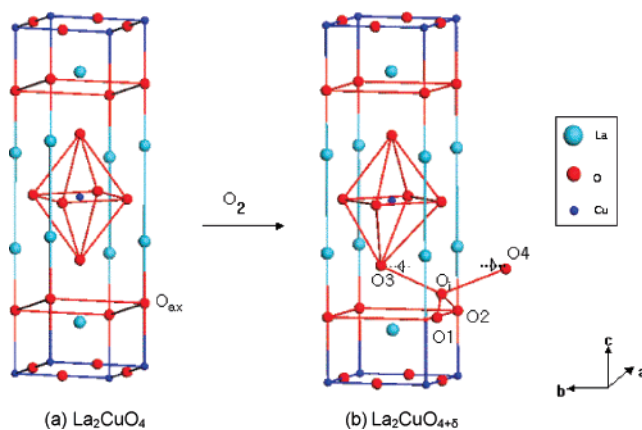


**Figure 1.** Structure of the  $\text{La}_2\text{CuO}_4$  material (pristine and interstitial oxygen structures): (a) One tetragonal unit cell is represented. (b) The position of interstitial oxygen is represented by  $\text{O}_i$ . The La and O1 positions are not affected by the presence of the  $\text{O}_i$  excess oxygen. The excess oxygen brings about the displacement of the O1 oxygen atoms toward the O3 sites, and the movement is represented by the dotted lines.

defect is observed in the absorption peak with the lowest activation enthalpy, which is visible at the lowest values of doping and is attributed to the hopping of single interstitial ions. The second process of defect formation, which has slightly slower dynamics, appears at the highest value of  $\delta$  and soon dominates over the former. The latter process is proposed to be due to stable pairs of O atoms, the outcome of the formation of partially covalent bonds between interstitial and apical oxygens. Using the pressure–composition curve determined at 823 K, an analysis of the partial desorption stages indicates the possibility of the formation of interstitial  $\text{O}^{2-}$  ions and suggests the possibility of the formation of peroxide or superoxide species.<sup>19</sup>

Radaelli and co-workers<sup>20</sup> studied two powder samples of electrochemically oxidized  $\text{La}_2\text{CuO}_{4+\delta}$  ( $\delta = 0.08$  and  $0.12$ ) and one single crystal ( $\delta = 0.1$ ) with superconducting critical temperatures of 32, 42, and 40 K, respectively, using neutron diffraction, thermogravimetric analysis (TGA), and iodometric titration. The basic crystallographic structure of all samples has  $Fm\bar{3}m$  symmetry, with the excess oxygen located between adjacent LaO layers. TGA data and iodometric titration suggest  $\text{O}_2^{2-}$  in the material.

### Theoretical Work

Many calculations have been made on the ideal  $\text{La}_2\text{CuO}_4$  system, by both band structure<sup>21</sup> and molecular cluster methods.<sup>22–25</sup> In studying oxygen doping, quantum chemical calculations on cluster models of  $\text{La}_2\text{CuO}_{4+\delta}$  were carried out in order to interpret one of two satellite peaks of the copper Nuclear Quadrupole Resonance (NQR) spectra.<sup>26–28</sup> The self-consistent discrete variational method with a local density functional formalism<sup>17</sup> was used to select the proper interstitial site from three models of a fragment consisting of  $N$  ( $N = 30–44$ ) atoms embedded in the infinite crystal. It was found that the charge on the oxygen dimer, which is located in these calculations perpendicular to the Cu–O–Cu axis in the  $\text{CuO}_2$  plane, is consistent with that of normal oxide,  $-2$  per oxygen. The single-crystal neutron diffraction studies,<sup>4–6</sup> however, suggest that interstitial oxygen atoms are sandwiched between two successive La–O layers (see Figure 1).

### The Central Problem: Do We Have $\text{O}^{2-}$ , $\text{O}^-$ , $\text{O}$ , $\text{O}_2^{3-}$ , $\text{O}_2^{2-}$ , $\text{O}_2^-$ , or $\text{O}_2$ ?

This summary of much excellent experimental and theoretical labor shows that there is hardly a consensus on the nature of

interstitial oxygen in the cuprates. Two properties of these superconductors make, however, the question of the oxygen central to their nature and we believe to the phenomenon of high temperature superconductivity: (a) Oxygen doping is a reality. The critical nonstoichiometries allow movement of oxygen from  $\text{O}_2$  in the gas to formal  $\text{O}^{2-}$  in the solid. (b) All electronic structure calculations point to holes partially on copper, partially on oxygen (therefore, what was formally  $\text{O}^{2-}$  becoming  $\text{O}^-$  or even O) in the cuprate layers. To a chemist, a hole on an oxide is a source of reactivity. What does that hole do?

Thus, we are interested in understanding whether the interstitial oxygen atoms<sup>10,15–19</sup> are O,  $\text{O}^-$ , or  $\text{O}^{2-}$ . If we take the hole on the oxide in a chemical sense as  $\text{O}^-$ , one would expect such  $\text{O}^-$  species<sup>10</sup> to bond with an oxide ( $\text{O}^{2-}$ ) ion, to bond with another  $\text{O}^-$ , or to interact in some way with molecular oxygen ( $\text{O}_2$ ). The products of such reaction might be superoxide ( $\text{O}_2^{3-}$ ), peroxide ( $\text{O}_2^{2-}$ ), or superoxide ( $\text{O}_2^-$ ) diatomic species, existing as defects in the lattice or product species on the surface. Just as in the case of a Jahn–Teller distortion, such dimerizations may be real (static distortion) or manifest themselves as softened vibrational modes.

In this paper, we present a detailed theoretical analysis of the formation of  $\text{O}_2^{q-}$  ( $q = \text{integer}$ ) entities in  $\text{La}_2\text{CuO}_4$ . We will propose a relationship between the geometrical positions of interstitial oxygen and the experimental properties of the cuprates, such as the stripe pattern of interstitials and the change of the slope of hole concentration versus excess oxygen content.<sup>14</sup>

We will also analyze the effect of antiferromagnetic (AF) and magnetic backgrounds on the model clusters. This is necessary because an increasing density of holes causes the background antiferromagnetism to become less dominant, and impurities can break the delicate balance that allows the magnetism of each atom to be neutralized through singlet formation. All of our explanations are based on both the theoretical valences and spin densities of interstitial oxygen atoms obtained from quantum chemical calculations on cluster models of  $\text{La}_2\text{CuO}_{4+\delta}$ .

### Model Clusters and Computational Details

In our cluster models for  $\text{La}_2\text{CuO}_{4+\delta}$ , the solid is approximated using a Madelung–Pauli embedding potential.<sup>22</sup> Here, all electrons in the primary core cluster of the embedding cluster model are treated by *ab initio* all-electron methods. The primary core cluster is surrounded by basis-free pseudopotentials and, at a farther distance, simple point charges at the atomic sites of the lattice. We use basis-free pseudopotentials on the  $\text{Cu}^{2+}$  and  $\text{La}^{3+}$  sites in order to enforce orthogonality between the electrons in the primary cluster and the point charges of background ion sites.

The undoped  $\text{La}_2\text{CuO}_4$  crystal is modeled by two primary  $\text{Cu}_2\text{O}_{11}$  clusters and two secondary  $\text{La}_{12}\text{Cu}_6$  clusters in a lattice of 5666 point charges (PC); we call this  $2(\text{Cu}_2\text{O}_{11}/\text{La}_{12}\text{Cu}_6)/5666\text{PC}$ . In this model, the primary  $\text{Cu}_2\text{O}_{11}$  cluster is treated with an all-electron basis set, while the 12 surrounding Cu ions and 24 La ions are represented by bare pseudopotentials. The  $\text{Cu}_2\text{O}_{11}/\text{La}_{12}\text{Cu}_6$  unit is shown in Figure 2. There is no interstitial oxygen at this stage of modeling.

The  $2(\text{Cu}_2\text{O}_{11})/\text{O}_7/2(\text{La}_{12}\text{Cu}_6)$  structure is the model cluster for the interstitial O atom in the cuprate. It is shown in Figure 3. This model cluster has  $D_{2d}$  symmetry and has in it parts of two Cu layers. All atoms are located according to their positions in the tetragonal phase, with lattice constants of  $a = 3.801 \text{ \AA}$  and  $c = 13.148 \text{ \AA}$ , with a Cu–O (apex) distance of  $2.401 \text{ \AA}$ .

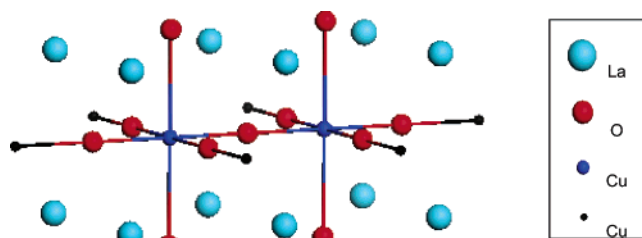


**Figure 2.**  $\text{Cu}_2\text{O}_{11}/\text{La}_{12}\text{Cu}_6$ : The core  $\text{Cu}_2\text{O}_{11}$  cluster is shown connected by lines; the surrounding ions are  $\text{La}_{12}\text{Cu}_6$ .

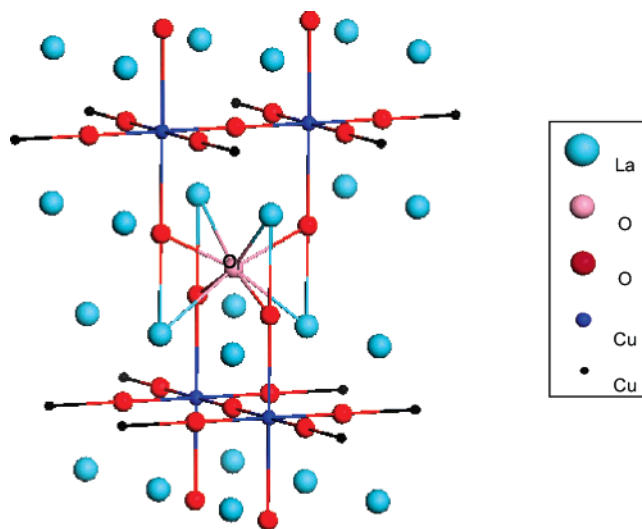


**Figure 3.**  $2(\text{Cu}_2\text{O}_{11})/\text{O}_7/2(\text{La}_{12}\text{Cu}_6)$ : Two  $\text{Cu}_2\text{O}_{11}/\text{La}_{12}\text{Cu}_6$  clusters surround an interstitial oxygen atom in this model. The Cu atoms in the first and secondary clusters are distinguished by the different colors and sizes of the circles.

The value of the lattice constant ( $a$ ) is chosen as the average of the lattice constants ( $a$  and  $b$ ) of the structure obtained from the single-crystal neutron diffraction study of Chaillout and co-workers.<sup>5</sup>

The point charge field that surrounds the primary and secondary cluster is generated by replicating the basic unit. Formal ionic charges of +2, –2, and +3 are assigned to Cu, O, and La, respectively. The ions at the periphery of the basic cell, which are shared by more than one cell, are taken to carry an appropriate fractional charge, so that the total charge in the basic unit is zero.

Various approximations to the Madelung potential are generated by translating the basic unit cell along the  $x$ ,  $y$ , and  $z$  axes. Let's denote these ion arrangements by the number of cells in each direction. Thus, if the basic cell is  $1 \times 1 \times 1$ , the collection of ions obtained when this cell is translated forward and backward one unit along the  $x$  axis is  $3 \times 1 \times 1$ . Then, the lattice of 5666 point charges which serve as the embedding "background" may be labeled as  $10 \times 10 \times 7/2$ . When we increase systematically the finite lattice point charge background from  $3 \times 3 \times 3$  to  $10 \times 10 \times 10$  in size, we get a consistent charge at the interstitial oxygen in the center of our model cluster from  $6 \times 6 \times 7/2$  on. For the noninterstitial oxygen atom, a consistent charge is obtained from  $6 \times 6 \times 3$  on. That is the reason we chose  $10 \times 10 \times 7/2$  as a background size for embedding.

All electrons on the Cu ions were considered explicitly using a  $[6s/5p/3d]$  contraction of Wachters' primitive basis for Cu.<sup>29</sup> The standard 6-31G\* basis set was used for the O atom. The effective core potentials of Martin and Hay<sup>22</sup> were used to represent the 12  $\text{Cu}^{2+}$  sites and 24  $\text{La}^{3+}$  sites that immediately

**TABLE 1: Relative Energies, Atomic Charges, and Spin Densities (in Parentheses) of an Interstitial Oxygen ( $O_i$ ) and Its Nearest Neighbor Copper and Oxygen Atoms<sup>a</sup>**

total spin	model	$\Delta E$ (meV) <sup>b</sup>	atomic charge (spin density)								
			Cu1	Cu2	Cu3	Cu4	O1	O2	O3	O4	$O_i$
0	A	234	0.80 (0.61)	-0.62	0.62	-0.61	-1.63 -0.24	-0.23	0.23	0.24	-1.00 (0.00)
	B2	292	0.80 (0.61)	-0.62	-0.61	0.61	-1.63 -0.24	-0.23	-1.64	0.23	-0.99 (0.00)
	B1	1160	0.73 (-0.56)	0.81 0.61	0.78 -0.61	0.61	-1.27 -0.01	-1.65 0.00	-1.85	-1.84	-0.96 (0.00)
1	A	0	0.80 (-0.61)	0.62	-0.61	0.62	-1.64 0.23				-0.95 (1.06)
	B2	57	0.80 (-0.61)	0.62	-0.61	0.61	-1.64 0.24	0.23	-1.65	0.22	-0.95 (1.06)
	B2	434	0.81 (0.65)	0.82 0.61	0.78 -0.61	0.61	-1.63 -0.23	-1.65	-1.64	0.23	-0.99 (0.00)
	B1	1327	0.75 (0.61)	0.82 0.65	0.78 0.61	-0.61	-1.27 0.00	-1.65	-1.85	-1.84	-0.96 (-0.01)
2	A	134	0.80 (-0.61)	0.62	0.81	0.62	-1.64 0.23				-0.95 (1.06)
	B2	190	0.80 (-0.61)	0.62	0.81	0.62	-1.64 0.24	0.23	-1.65	0.22	-0.95 (1.06)
	B1	1441	0.75 (0.61)	0.82 0.65	0.79 0.64	0.79	-1.27 0.00	-1.65	-1.85	-1.84	-0.96 (0.00)
3	A	269	0.81 (0.65)				-1.64 0.23				-0.95 (1.06)
	B2	326	0.81 (0.65)				-1.64 0.23		-1.65	0.22	-0.95 (1.06)
	B1	2948	0.75 (0.66)	0.81 0.64	0.80 0.63	0.79	-1.41 0.47	-1.49 0.41	-1.80 0.08	-1.77 0.09	-1.09 (0.90)
Without Oxygen Doping											
0		0	0.79 (-0.62)	0.62	-0.62	0.62	-1.87 0.00				)
2		263	0.80 (0.65)				-1.87 0.00				)

<sup>a</sup> These are computed by UB3LYP calculations for specified constrained spin of several model clusters (A, B1, and B2) with a different local environment of  $O_i$ . The model cluster is  $Cu_4O_{22}/O_i/Cu_{12}La_{24}/5666$  point charges in a  $(10 \times 10 \times 7/2)$  cell cubic box. The value of each blank cell is the same as that of the one on its left. <sup>b</sup> Reference energies (atomic units):  $E(S=1) = -12\,849.6844$  with interstitial O and  $E(S=0) = -12\,774.5473$  without interstitial O in UB3LYP calculations.

adjoin the primary cluster. All calculations were performed with the Gaussian 98 suite of programs.<sup>30</sup> We have performed unrestricted hybrid B3LYP (UB3LYP) calculations on cluster models. In the density functional theory (DFT) calculations, we use the notation B3LYP to refer to Beck's three-parameter hybrid functional,<sup>31</sup> combined with the correlation functional of Lee, Yang, and Parr.<sup>32</sup>

### The Three Models

Three different local environments of interstitial oxygen were used to simulate various experimental situations. When an interstitial oxygen atom is at the center of the model cluster,  $2(Cu_2O_{11})/O_i/2(La_{12}Cu_6)$ , this is called model A, which has  $D_{2d}$  symmetry. The local environment of  $O_i$  in model A is shown in Figure 4. Another possibility considered for the location of the interstitial oxygen is that suggested by the single-crystal neutron diffraction study of Chaillout and co-workers,<sup>5</sup> shown in Figure 1. If a local distortion of three of the nearest four oxygen atoms of this site (as shown in Figure 1) is allowed, the model is called B1 (see Figure 4). If such local distortions of the surrounding oxygens are not allowed, we have model B2 (also shown in Figure 4). Model clusters B1 and B2 have  $C_1$  and  $C_{2v}$  symmetry, respectively.

The  $2(Cu_2O_{11})/2O_i/2(La_{12}Cu_6)$  structure is a model cluster with two interstitial O atoms. Here, one interstitial oxygen atom is at the center. The other oxygen occupies the site corresponding to one of four nearest neighbor central sites given by translational symmetry in the bulk. We will call this the "interstitial pair" (see Figure 5).

The computational results for models (A, B1, and B2) for a single interstitial oxygen atom under tetrahedral and reduced

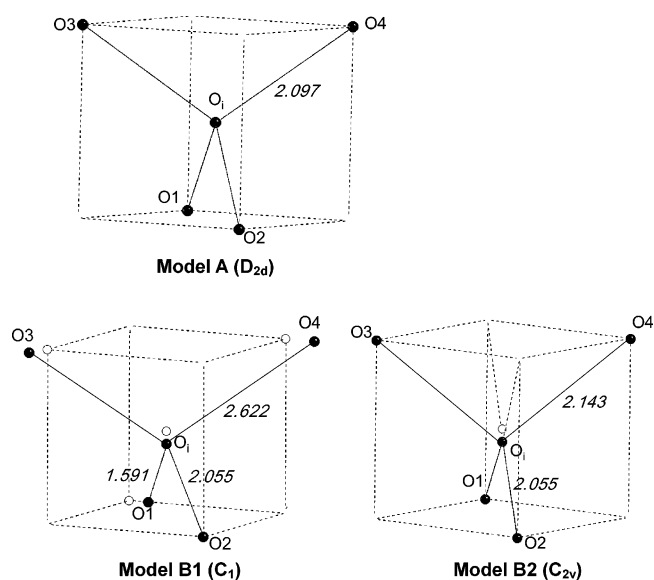


**Figure 4.** Structural environment of the four oxygen atoms closest to the interstitial oxygen. Each is the part of models A, B1, and B2, respectively. The local symmetry is in parentheses. Selected interatomic distances (angstroms) are shown in italics.

symmetry environments of its nearest neighbors (as shown in Figures 3 and 4) are presented in Table 1. Calculations for each model (A, B1, and B2) were carried out for a total spin of 0, 1, 2, and 3 in order to consider the effects on the interstitial oxygen atom of the electronic spins at the nearest neighbor atoms. The model of an oxygen interstitial pair (see Figure 5) in which an oxygen atom occupies one of four neighboring "central" sites

**TABLE 2: Relative Energies, Atomic Charges, and Spin Densities of an Interstitial Oxygen and Its Nearest Neighbor Copper and Oxygen Atoms of the Interstitial Pair as Calculated by the B3LYP Method<sup>a</sup>**

spin	$\Delta E$ (meV)	atomic charge (spin density)									
		Cu1	Cu2	Cu3	Cu4	O1	O2	O3	O4	O <sub>i</sub> 1	O <sub>i</sub> 2
UB3LYP Method											
0	663	0.79 (0.60)	0.80 -0.60	0.60	0.79 -0.60	-1.57 -0.31	-1.35 0.25	-0.25	-1.57 0.31	-0.97 0.00	-0.82 0.00
1	357	0.80 (0.61)	-0.60 0.60	0.60	0.79 -0.60	-1.60 0.29	-1.34 0.55	-1.35 -0.27	-1.59 0.30	-0.93 1.08	-0.82 0.02
2	0	0.80 (0.61)	-0.60 0.61	0.61	-0.60 0.28	-1.60 0.54	-1.36 0.54	-1.36	-1.60 0.29	-0.94 1.08	-0.77 1.22
3	131	0.81 (0.65)	0.64 0.61	0.61	-0.60 0.28	-1.60 0.54	-1.36	-1.60	-1.60 0.29	-0.94 1.08	-0.77 1.22
4	265	0.81 (0.65)	0.64	0.65	-1.60 0.28	-1.36 0.54	-1.36	-1.60	-1.60 0.28	-0.94 1.08	-0.77 1.22
ROB3LYP Method											
2		0.80 (0.69)	0.81 0.67	0.74 0.01	0.73	-1.60 0.28	-1.36 0.15		-1.60 0.27	-0.93 1.07	-0.87 0.03

<sup>a</sup> The spin to which the model cluster  $\text{Cu}_4\text{O}_{22}/2\text{O}_i/\text{Cu}_{12}\text{La}_{24}/5666$  point charges in a  $(10 \times 10 \times 7/2)$  cell cubic box is constrained is specified. The value of any blank cell is the same as that of the one on its left. <sup>b</sup> Reference energies (atomic units) with two interstitial O atoms:  $E(S=2) = -12\,924.8297$  in UB3LYP calculations.

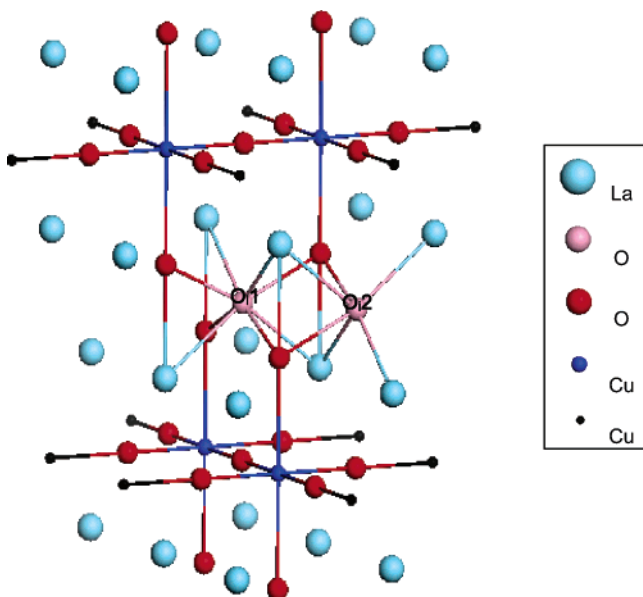


**Figure 5.**  $2(\text{Cu}_2\text{O}_{11}/2\text{O}_i/2(\text{La}_{12}\text{Cu}_6))$ : In this model, two  $\text{Cu}_2\text{O}_{11}/\text{La}_{12}\text{Cu}_6$  clusters surround two interstitial oxygen atoms ( $\text{O}_{i1}$  and  $\text{O}_{i2}$ ), which are in the tetrahedral symmetry environment given by four La atoms of two secondary  $\text{La}_{12}\text{Cu}_6$  clusters. In addition,  $\text{O}_{i1}$  is in a tetrahedral environment of four oxygen atoms of two primary  $\text{Cu}_2\text{O}_{11}$  subclusters, while  $\text{O}_{i2}$  is in the same environment formed by two oxygen atoms of two primary  $\text{Cu}_2\text{O}_{11}$  clusters and two formal oxygen point charges.

closest to the occupied central site of model cluster A (compared to two separate single interstitials) is analyzed in Table 2. For the case of an oxygen interstitial pair, only model A is considered, with the spin ranging between 0 and 4.

## Results and Discussion

We first focus on the “magnetic moment”, as determined by the Mulliken unpaired spin population on the metal site, since the spin unrestricted solutions are also eigenfunctions of  $\hat{S}_z$ . Let’s consider the  $2(\text{Cu}_2\text{O}_{11}/\text{La}_{12}\text{Cu}_6)/5666\text{PC}$  results in Table 1. The UB3LYP and unrestricted Hartree–Fock (UHF, not shown in Table 1) unpaired spin populations on the Cu sites are calculated to be 0.62 and 0.88, respectively, indicating a sizable magnetic moment. These populations are similar to the spin value 0.83 inferred from the observed moment  $0.5 \mu\text{B}$ .<sup>33</sup> The remainder of the unpaired spin is delocalized onto the oxygen  $2p_\sigma$  orbitals. Generally, the UHF approximation overestimates the degree of

spin localization, while UB3LYP underestimates it.<sup>23,24</sup> Our results agree with the work reported by Martin and Illas,<sup>23,24</sup> who get 0.90 (UHF)<sup>23</sup> and 0.68 (UB3LYP)<sup>24</sup> with  $\text{Cu}_2\text{O}_{11}$  cluster models. Both the UHF and UB3LYP approximations correctly reproduce the antiferromagnetic behavior of  $\text{La}_2\text{CuO}_4$ .

The role of interstitial oxygen in  $\text{La}_2\text{CuO}_{4+\delta}$  is curious, because interstitial oxygen induces a structural phase transition in superconducting  $\text{La}_2\text{CuO}_{4+\delta}$ . To understand the valence state of the interstitial oxygen atom, we also calculated the Mulliken atomic charges and relative energies of a  $2(\text{Cu}_2\text{O}_{11}/\text{La}_{12}\text{Cu}_6)/5666\text{PC}$  model cluster with and without interstitial oxygen atoms. The charge and spin densities of the interstitial ( $\text{O}_i$ ) and neighbor atoms in models A, B1, and B2 for a separate single interstitial and their relative stability are shown in Table 1. The relative stability of the interstitial pair is calculated from the data in Tables 1 and 2.

The interstitial pair energy is 18 meV. This is computed as the energy of an interstitial pair (with  $S = 2$ ) formed by filling one of four neighbor central sites nearest to the occupied central site, compared to two separate single interstitials of model cluster A with  $S = 1$ . In our models, the two interstitial sites in the interstitial pair have a different electrical field environment. The energy of model A with a single interstitial is higher (241 meV) than one in the local environment of the nearest two oxygen atoms and two oxygen point charges ( $-2$ ) for two interstitial sites. That there are two different local environments for the interstitial site is a consequence of the limited size of the model cluster.

We also see the effect of constraining the spin with interstitial oxygen monomer and interstitial pair models in Tables 1 and 2, respectively. An antiferromagnetic background is modeled by  $S = 0$ , for a zero spin of an interstitial oxygen atom. The  $S = 1$  case models a state with two unpaired electrons on the  $\text{O}_i$  atom in Table 1. States with  $S = 2$  and 3 model a ferromagnetic background, depending on the value of the initial spin state of the oxygen atom.

Recent NQR spectra simulations have not considered the spin state of the interstitial oxygen.<sup>26,27</sup> Thus, it is interesting to examine the effect of interstitial spin on the charge and spin density of the interstitial and neighbor atoms. The labeling of copper and oxygen atoms in Tables 1 and 2 is the same as that in Figure 1, just as the numbering of each copper atom bonded to the axial oxygen atom follows the numbering of each oxygen atom.

The theoretical results, shown in Table 1, indicate that the valence state of the interstitial oxygen is about  $-1.0$  for all

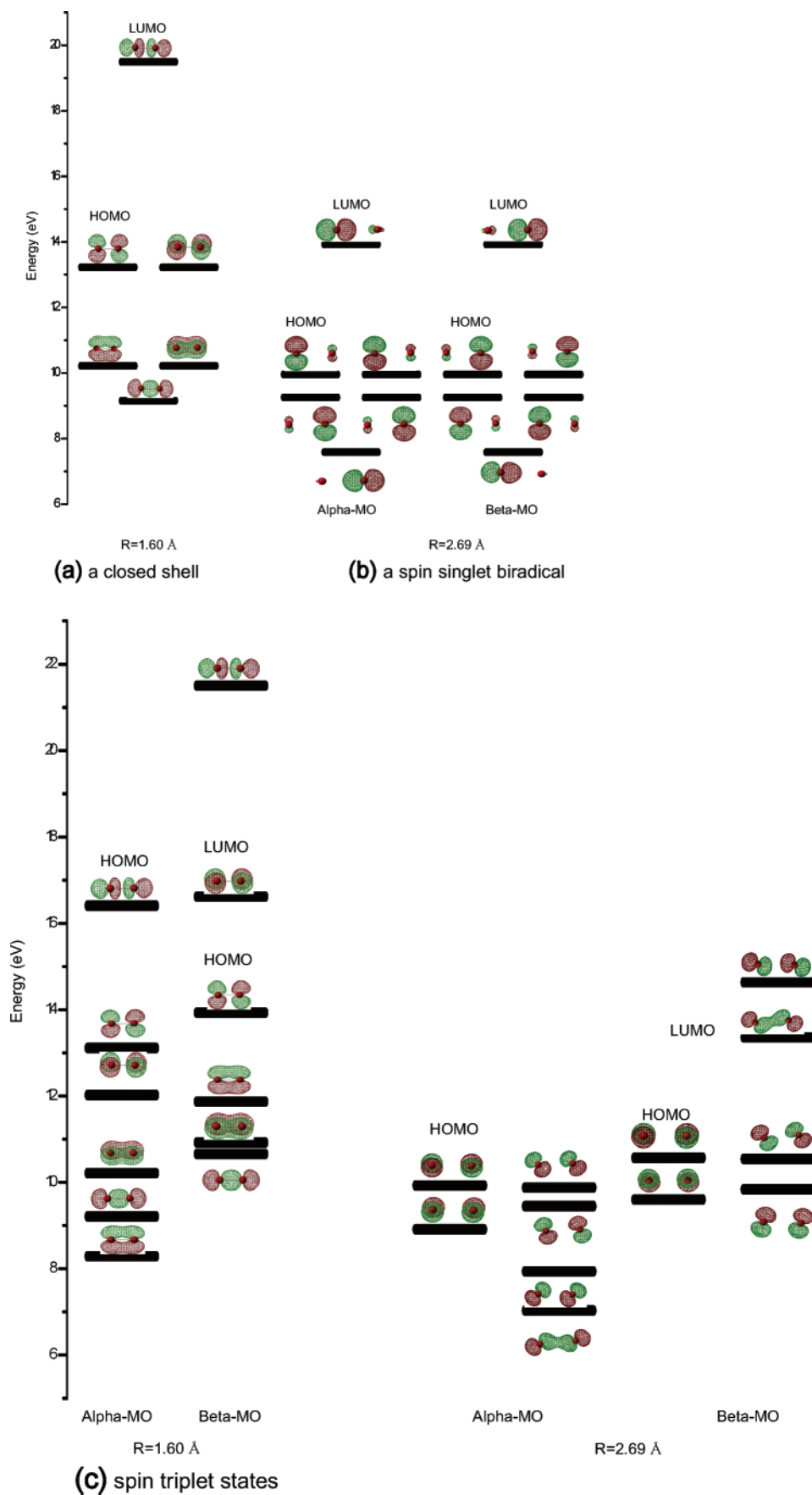


**Figure 6.** Assembly of the orbital diagram for peroxide at O–O distances of 1.60 and 2.69 Å, respectively. The oxygen sites are represented by the closed red circles. Here, we show (a) a closed shell singlet MO at  $R = 1.60 \text{ \AA}$ , (b) a spin singlet biradical state at  $R = 2.69 \text{ \AA}$ , and (c) spin triplet states at  $R = 1.60$  and  $2.69 \text{ \AA}$ .

model clusters (A, B1, and B2). This holds approximately for all of the total constrained spin states calculated ( $S = 0-3$ ) of all the model clusters. The implication is that the valence of the interstitial oxygen atom is independent of the magnetic background, and an interstitial oxygen atom derives one electron from the copper oxide. Our calculations thus support the existence of the  $\text{O}^-$  ion in the cuprates, as observed in X-ray photoelectron spectroscopic (XPS) and magnetization studies.<sup>10</sup>

The stable  $\text{O}^-$  species obtained in our calculations allows us to suggest a mechanism for the evolution of oxygen in  $\text{La}_2\text{CuO}_{4+\delta}$ : two  $\text{O}^-$  states can produce peroxide ( $\text{O}_2^{2-}$ ), and then, two peroxide ( $\text{O}_2^{2-}$ ) species could react further to make  $2\text{O}^{2-}$  and  $\text{O}_2$ . This mechanism, while quite tentative, may explain a variety of experimental results.<sup>10-13,20</sup>

The signs of the computed copper spin densities in Table 1 suggest that this UB3LYP approach to our models may mimic the antiferromagnetic, ferrimagnetic, and ferromagnetic phases for  $\text{La}_2\text{CuO}_{4+\delta}$ . The description of antiferromagnetic coupling in  $\text{La}_2\text{CuO}_4$  is satisfactory, as the calculated  $J$  value ( $\sim 132$  meV) is within 3% of the experimental value (128 meV) of  $\text{La}_2\text{CuO}_4$ .<sup>24</sup>

In model clusters A and B2, the energy associated with a spin flip at the Cu site of  $S = 1$  and 2 is about half of that of  $S = 1$  and 3 (less than 0.8% difference), implying that there is very weak  $\text{Cu}^{2+}-\text{Cu}^{2+}$  magnetic coupling between two successive layers of copper oxides. This very weak interaction ( $\sim 1$  meV), however, would suggest that the spin flips at Cu sites in two successive copper oxide layers could be opposite.

The calculated  $J$  value (134 meV) is (for all spin states) about 2.5 times the displacement energy (about 57 meV) of  $\text{O}_i$  involved in the transformation of model A into model B2. The annihilation of electron spin density of the interstitial oxygen atom requires about 234 meV (see relative energy in Table 1), which is higher than the  $\text{Cu}^{2+}-\text{Cu}^{2+}$  magnetic coupling constant.

The local spin density of interstitial oxygen is calculated to be around 1.1 in model clusters A and B2 with constrained spins  $S = 1-3$ . It is 0.0 for all model clusters with constrained spin  $S = 0$ . For model cluster B1, it is 0.0 in the case of constrained spins  $S = 1$  and 2, while it is 0.9 for  $S = 3$ . The calculated energies of model clusters A and B2 (shown in Tables 1 and 2) are lower if interstitial oxygen carries the local spin density, compared to the case when it does not. This implies that the electron spin density of interstitial oxygen is important to the relative stability of the system. This paramagnetic interstitial oxygen species could explain isolated paramagnetic spins in the experimental magnetization data of  $\text{La}_2\text{CuO}_{4+\delta}$ .<sup>9,10,12</sup>

In model B1, the interstitial oxygen ( $\text{O}_i$ ) essentially forms a bond (1.59 Å) with the  $\text{O}_1$  that is one of the oxygen atoms lying at the apex of the four nearby  $\text{CuO}_6$  octahedra (see Figures 1 and 4). As the  $\text{O}_1$  bonds to the  $\text{O}_i$ , the  $\text{Cu}-\text{O}_1$  bond length increases from 2.401 to 2.503 Å. Bond formation between  $\text{O}_i$  and  $\text{O}_1$  reduces the  $D_{2h}$  local symmetry environment around the interstitial oxygen atom to  $C_1$ . Inspection of the distances shown in Figure 4 indicates that there must still be some bonding interaction of  $\text{O}_i$  with  $\text{O}_2$  (2.055 Å away), but we essentially have a strong  $\text{O}_i-\text{O}_1$  covalent bond of the peroxide type, with a formal charge of  $-2$  and a spin naught state. This we call the "covalent dimer" (see Figures 1 and 4), interacting with the lattice oxygen<sup>9,10</sup> in  $\text{La}_2\text{CuO}_{4+\delta}$ .

The energy difference between  $S = 0$  and  $S = 1$  is 167 meV, while the energy difference between the  $S = 1$  and  $S = 2$  states is 114 meV, which represents the effect of background magnetic properties. If the interstitial O were a doublet  $\text{O}^-$  coupling with a lattice oxide ( $\text{O}^{2-}$ ), one would get  $S = 1/2$  for a resulting superperoxide ( $\text{O}_2^{3-}$ ). This would be the state of model cluster B1 with  $S = 3$ . However, our calculations make this a very

high energy state, in which the interstitial O carries electron spin density ( $=0.9$ ), compared to the spin zero state of  $\text{O}_i$  in model B1 with  $S = 0, 1$ , and 2. Thus, our results support the idea that in a heavy doping situation the interstitial oxygen atoms could interact with lattice oxides to form a peroxide  $\text{O}_2^{2-}$  state.<sup>5,19,20</sup>

Model cluster A of  $\text{La}_2\text{CuO}_{4+\delta}$  (shown in Figure 5) has two interstitial oxygen atoms, what we call an interstitial pair model. At the UB3LYP level, we get only a peroxide state for an interstitial oxygen pair, over the range of constrained local spins from  $S = 0$  to  $S = 4$  in  $\text{La}_2\text{CuO}_{4+\delta}$ , a conclusion derived from the computed sum of atomic charges on the interstitial oxygen species:  $-1.79, -1.75, -1.71, -1.71$ , and  $-1.71$ , respectively. Thus, our UB3LYP level calculations support that the interstitial oxygen atoms in this system are in a peroxide ( $\text{O}_2^{2-}$ ) state.<sup>19,20</sup>

The relative energies of model cluster B2 with  $S = 0-3$  show that the energy associated with a spin flip at a Cu site is lower ( $\sim 10$  meV) if interstitial oxygen has an electron spin density, compared to the case when it does not (see Table 1). The energy associated with a spin flip at the Cu site of  $S = 2$  and 3 in Table 2 is 131 meV, which is almost the same value ( $=134$  meV) as that derived from the change of total spin from  $S = 1$  to  $S = 2$  in model cluster A in Table 1. The energy associated with a spin flip at a Cu site in model B1 (by changing from  $S = 1$  to  $S = 2$ ) goes down by about 15%, which suggests that increasing the oxygen doping concentration could decrease the Néel temperature of this system. Here, the interstitial oxygen forms bonds with the axial oxygen,  $\text{O}_1$ , to form a peroxide, which does not carry spin density. As far as we know, this is the first ab initio calculation to estimate the change in energy associated with a spin flip at a Cu site by the interstitials.

As shown in Tables 1 and 2, both the charge and spin densities of  $\text{O}_1, \text{O}_2, \text{O}_3$ , and  $\text{O}_4$  (compared to the case when the oxygen interstitial is not doped) show a loss of about 0.23 electrons and a gain of 0.23 spin density. Thus, this tetrahedron of oxygen atoms nearest to the interstitial oxygen could form both charge and spin density stripes.

A word on stripes: Various experimental studies have demonstrated that antiferromagnetism survives in the doped cuprates. At the same time, however, superconductivity requires mobile charge carriers. The competing electronic interactions between mobile holes and local antiferromagnetism coexisting in the copper oxide planes can lead to spatial segregation of the holes. Neutron and X-ray diffraction studies on variants of lanthanum cuprate have shown that this segregation takes the form of regularly spaced stripes of charge separating the antiferromagnetic domains. Prostripers have argued that the tendency toward charge segregation plays a crucial role in the hole-pairing mechanism essential to the superconductivity. On the other hand, sceptics have suggested that stripe order is a competing ground state, incompatible with superconductivity.<sup>3,7,8,35</sup>

We find that without any change of the local structural environment around the oxygen interstitials, the hole doping to the copper oxide layer comes only through the formation of an oxygen interstitial pair (ROB3LYP calculations with  $S = 2$ ). The hole doping to the copper oxide layer does not derive, so our calculations imply, from any change of the local structural environment and magnetic field around the single interstitial.

We believe our calculations support a chemically based finding that supports the underlying physics and chemistry of a stripe phase in high temperature superconductivity.

Paramagnetic spins were observed in the experiments of Schirber and co-workers,<sup>9</sup> where magnetization data show evidence for localized isolated spins at  $\text{La}_2\text{CuO}_{4+\delta}$ . These researchers used the presence of such paramagnetic spins to

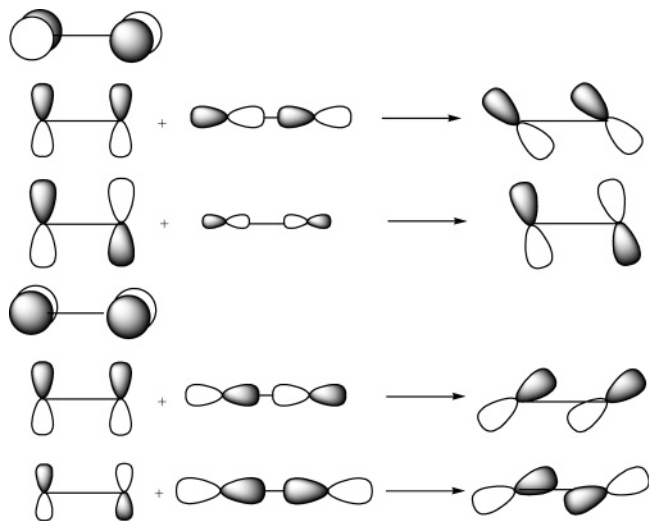


**Figure 7.** At long O–O separation, mixing occurs between inversion center symmetry-adapted canonical MOs appropriate to shorter distances. The phase of the orbital coupling between the  $\sigma^*$  antibonding and  $\pi$  bonding (and between the  $\sigma$  bonding and  $\pi^*$  antibonding) spin-orbitals is shown here.

argue for the existence of superoxide  $\text{O}_2^-$  ions comprised of interstitial oxygen atoms in this ceramic, since such paramagnetic spins could arise from superoxide ions or molecular oxygen but not from oxygen present as  $\text{O}^{2-}$  or  $\text{O}_2^{2-}$ .

If the  $\text{O}_2^{2-}$  were in the gas phase in its equilibrium state (short O–O distance, compared to the distance in the crystal system), their analysis would be right. A normal, molecular peroxide ion ( $\text{O}_2^{2-}$ ) would be a singlet ground state, with the  $\pi^*$  molecular orbital (MO) occupied by four electrons. The peroxide ( $\text{O}_2^{2-}$ ) state in our B3LYP calculations, however, has two unpaired electrons.

How can one have a high spin ground state for such a species? Reconciliation of this chemical notion with our calculations comes in several stages.

First, orbital diagrams for the normal orbitals of peroxide at a O–O distance of 1.60 Å and those for an O–O distance of 2.69 Å (obtained from the B3LYP calculations) are in Figure 6. The lowest energy state of peroxide is a spin singlet (diamagnetic) state with a closed shell at the short O–O distance, while it is a broken symmetry state with an open shell singlet (which a chemist would call a biradical) at the long O–O distance, as shown in Figure 6.

How does this happen? As the O–O bond stretches, the  $\sigma^*$  orbital of peroxide comes down in energy and into the region of the  $\pi^*$  MO. The spin triplet state we calculate has a hole in the  $\pi^*$  MO and one electron in  $\sigma^*$  MO at the long O–O distance (2.69 Å). This novel triplet state has a lower energy than the diamagnetic spin singlet state at the short O–O distance. Symmetry breaking is important here. This increased stability comes from configurational mixing at the long O–O distance (Figure 7).

The tilting of the orbitals in the UB3LYP calculations comes from configuration mixing between the following two configurations for  $\text{O}_2^{2-}$ : (a)  $\sigma_{2s}^2 \sigma_{2s}^* \sigma_{2p}^2 \pi_{2p}^4 \pi_{2p}^* \sigma_{2p}^*$  and (b)  $\sigma_{2s}^2 \sigma_{2s}^* \sigma_{2p}^2 \pi_{2p}^4 \pi_{2p}^*$ . In other words, the UB3LYP methodology includes correlation, and this leads to the mixing of orbital pairs  $\sigma_{2p} - \pi_{2p}^*$  (HOMO-3–HOMO) and  $\pi_{2p} - \sigma_{2p}^*$  (HOMO-1–LUMO) at 2.69 Å. Here, we use the highest occupied molecular orbital (HOMO) and lowest unoccupied molecular orbital (LUMO) notation referring to the orbitals at 1.60 Å. The weakened interaction between O atoms at 2.69 Å transforms a delocalized MO picture into a more atomic one. A valence bond

(VB) description of this change (always better near dissociation) might be appropriate.

Our UB3LYP calculations (in the crystal field of point charges) say that the energy of the broken symmetry state of the interstitial oxygen pair is almost the same as the triplet state. Thus, our results suggest that the paramagnetic state of the interstitial oxygen pair could arise from electron correlation of the acting in the weakened interaction of relatively distant interstitial oxygen atoms (see the spin density of the interstitial oxygen pair in Table 2).

The last thing to be explained is the change of the slope (from 2 to 1.3) of hole concentration versus excess oxygen content.<sup>14</sup> This phenomenon can also be understood by using the ROB3LYP calculations. We find that model cluster B1 is more stable than model cluster B2, which in turn is more stable than model A. These results are in agreement with ref 27. In the model clusters of oxygen-doped  $\text{La}_2\text{CuO}_4$ , however, the preferred site of the interstitial  $\text{O}_i$  is the central site, if  $\text{O}_i$  carries the local electron spin density. This means that the preferred site is heavily dependent on the local crystal structure environment and electron spin density of  $\text{O}_i$ .

Here, we can explain the change of the slope of hole concentration versus excess oxygen content by using the computed change in the local structure and electron spin density of interstitial oxygen, as one proceeds from model cluster A to model cluster B1. Because model cluster A can form a stripe of interstitial oxygen atoms sharing two axial oxygen atoms by two interstitial oxygen atoms, it has a greater degree of hole doping to the copper oxide layer than model B1. In the latter, it is almost impossible to get two axial oxygen atoms shared by two interstitial oxygen atoms.

Our calculations show that interstitial oxygen atoms make a peroxide bond with apical oxygen in model cluster B1. If the system is changed from insulator to metallic by oxygen doping, the slope of hole doping concentration should be decreased with an increase in the concentration of interstitial oxygen atoms. Bonding of apical oxygen with interstitial oxygen may deteriorate the conductivity of  $\text{La}_2\text{CuO}_{4+\delta}$ .

In summary, our calculations indicate that the interstitial oxygen atoms in  $\text{La}_2\text{CuO}_{4+\delta}$  should form peroxide ( $\text{O}_2^{2-}$ ) and  $\text{O}^-$  states. The experimentally observed paramagnetism could be explained by the localized electron spin density of interstitial oxygen ions. The energy associated with a spin flip at Cu sites decreases with increasing doping concentration, if the interstitial oxygen loses its electron spin density by bonding with the axial oxygen. This could explain why increasing the doping concentration of interstitial oxygen decreases the Néel temperature of this system. We also found that in models of a magnetic phase tetrahedron oxygen atoms nearest to the interstitial oxygen showed a pattern of a charge and spin density stripe. In contrast, models of a metallic phase gave a charge and hole stripe of tetrahedron oxygen atoms nearest to the interstitial oxygen.

**Acknowledgment.** We are grateful to Dr. Richard L. Martin, LANL, for helpful discussions and advice and to the National Science Foundation for its support of the work at Cornell through research grant CHE-0204841.

## References and Notes

- (1) Bednorz, G.; Müller, K. A. *Z. Phys. B* **1986**, *64*, 198. Axe, D.; Moudden, A. H.; Hohlwein, D.; Cox, D. E.; Mohanty, K. M.; Moodenbaugh, A. R.; Xu, Y. *Phys. Rev. Lett.* **1989**, *62*, 2751. Torardi, C. C.; Subramanian, M. A.; Gopalakrishnan, J.; Sleight, A. W. *Physica C* **1989**, *158*, 465.
- (2) (a) Mattheiss, L. F. *Phys. Rev. Lett.* **1987**, *58*, 1028. (b) Yu, J. J.; Freeman, A. J.; Xu, J.-H. *Phys. Rev. Lett.* **1987**, *58*, 1035. (c) Whangbo, M.-H.; Evain, M.; Beno, M. A.; Williams, J. M. *Inorg. Chem.* **1987**, *26*, 1829. (d) Pickett, W. E. *Rev. Mod. Phys.* **1989**, *61*, 433.

- (3) Wells, B. O.; Lee, Y. S.; Kastner, M. A.; Christianson, R. J.; Birgeneau, R. J.; Yamada, K.; Endoh, Y.; Shirane, G. *Science* **1997**, *277*, 1067.
- (4) Jorgensen, J. D.; Dabrowski, B.; Pei, S.; Hinks, D. G.; Soderholm, L.; Morosin, B.; Schirber, J. E.; Venturini, E. L.; Ginley, D. S. *Phys. Rev. B* **1988**, *38*, 11337.
- (5) Chaillout, C.; Chenavas, J.; Cheong, S. W.; Fisk, Z.; Marezio, B.; Morosin, B.; Schirber, J. E. *Physica C* **1990**, *170*, 87. Chaillout, C.; Cheong, S. W.; Fisk, Z.; Lehmann, M. S.; Marezio, M.; Morosin, B.; Schirber, J. E. *Physica C* **1989**, *158*, 183.
- (6) Jorgensen, J. D.; Dabrowski, B.; Pei, S.; Richards, D. R.; Hinks, D. G. *Phys. Rev. B* **1989**, *40*, 2187.
- (7) Service, R. F. *Science* **1999**, *283*, 1106.
- (8) Tranquada, J. M.; Sternlieb, B. J.; Axe, J. D.; Nakamura, Y.; Uchida, S. *Nature (London)* **1995**, *375*, 561.
- (9) Schirber, J. E.; Morosin, B.; Merrill, R. M.; Hlava, P. F.; Venturini, E. L.; Kwak, J. F.; Nigrey, P. J.; Baughmann, R. J.; Ginley, D. S. *Physica C* **1988**, *152*, 121.
- (10) Rogers, J. W., Jr.; Shinn, N. D.; Schirber, J. E.; Venturini, E. L.; Ginley, D. S.; Morosin, B. *Phys. Rev. B* **1988**, *38*, 5021.
- (11) Zhou, J.; Sinha, S.; Goodenough, J. B. *Phys. Rev. B* **1989**, *39*, 12331.
- (12) Shin, N. D.; Rogers, J. W., Jr.; Schirber, J. E. *Phys. Rev. B* **1990**, *41*, 7241.
- (13) Strongin, M.; Qin, S. L.; Chen, J.; Lin, C. L. *Phys. Rev. B* **1990**, *41*, 7238.
- (14) Li, Z. G.; Feng, H. H.; Yang, Z. Y.; Hamed, A.; Ting, S. T.; Hor, P. H.; Bhavaraju, S.; DiCarlo, J. F.; Jacobson, A. J. *Phys. Rev. Lett.* **1996**, *77*, 5413.
- (15) Kieda, N.; Nishiyama, S.; Shinozaki, K.; Mizutani, N. *Solid State Ionics* **1991**, *49*, 85.
- (16) Hong, D. J. L.; Smyth, D. M. *J. Solid State Chem.* **1992**, *97*, 427.
- (17) Wu, Y.; Ellis, D.; Shen, L.; Mason, T. O. *J. Am. Ceram. Soc.* **1996**, *79*, 1599.
- (18) Cordero, F.; Grandini, C. R.; Cantelli, R. *Physica C* **1998**, *305*, 251.
- (19) Cordero, F.; Cantelli, R. *Physica C* **1999**, *312*, 213.
- (20) Radaelli, P. G.; Jorgensen, J. D.; Schultz, A. J.; Hunter, B. A.; Wagner, J. L.; Chou, F. C.; Johnston, D. C. *Phys. Rev. B* **1993**, *48*, 499.
- (21) Perry, J. K.; Tahir-Kheli, J.; Goddard, W. A., III. *Phys. Rev. B* **2001**, *63*, 144510.
- (22) Martin, R. L.; Hay, P. J. *J. Chem. Phys.* **1993**, *98*, 8680.
- (23) Martin, R. L.; Illas, F. *Phys. Rev. Lett.* **1997**, *79*, 1539.
- (24) Illas, F.; Martin, R. L. *J. Chem. Phys.* **1998**, *108*, 2519 and references therein.
- (25) Renold, S.; Heine, T.; Weber, J.; Meier, P. F. *Phys. Rev. B* **2003**, *67*, 024501.
- (26) Martin, R. L. *Phys. Rev. Lett.* **1995**, *75*, 744.
- (27) Plibersek, S.; Meier, P. F. *Europhys. Lett.* **2000**, *50*, 789.
- (28) Hammel, P. C.; Statt, B. W.; Martin, R. L.; Chou, F. C.; Johnston, D. C.; Cheong, S.-W. *Phys. Rev. B* **1998**, *57*, R712.
- (29) Wachtters, A. J. T. *J. Chem. Phys.* **1970**, *52*, 1033–1036. Russo, T. V.; Martin, R. L.; Hay, P. J. *J. Chem. Phys.* **1994**, *101*, 7729.
- (30) Frisch, M. J.; Trucks, G. W.; Schlegel, H. B.; Scuseria, G. E.; Robb, M. A.; Cheeseman, J. R.; Zakrzewski, V. G.; Montgomery, J. A., Jr.; Stratmann, R. E.; Burant, J. C.; Dapprich, S.; Millam, J. M.; Daniels, A. D.; Kudin, K. N.; Strain, M. C.; Farkas, O.; Tomasi, J.; Barone, V.; Cossi, M.; Cammi, R.; Mennucci, B.; Pomelli, C.; Adamo, C.; Clifford, S.; Ochterski, J.; Petersson, G. A.; Ayala, P. Y.; Cui, Q.; Morokuma, K.; Malick, D. K.; Rabuck, A. D.; Raghavachari, K.; Foresman, J. B.; Cioslowski, J.; Ortiz, J. V.; Stefanov, B. B.; Liu, G.; Liashenko, A.; Piskorz, P.; Komaromi, I.; Gomperts, R.; Martin, R. L.; Fox, D. J.; Keith, T.; Al-Laham, M. A.; Peng, C. Y.; Nanayakkara, A.; Gonzalez, C.; Challacombe, M.; Gill, P. M. W.; Johnson, B.; Chen, W.; Wong, M. W.; Andres, J. L.; Gonzalez, C.; Head-Gordon, M.; Replogle, E. S.; Pople, J. A. *Gaussian 98*, revision A.9; Gaussian, Inc.: Pittsburgh, PA, 1998.
- (31) Becke, A. D. *J. Chem. Phys.* **1993**, *98*, 5648.
- (32) Lee, C.; Yang, W.; Parr, R. G. *Phys. Rev. B* **1988**, *37*, 785.
- (33) Birgeneau, R. J.; Shirane, G. In *Physical Properties of High Temperature Superconductors*; Ginsberg, D. M., Ed.; World Scientific: Singapore, 1989; Vol. 1, p 151.
- (34) Chen, C. Y.; Branlund, E. C.; Bae, C.; Yang, K. *Phys. Rev. B* **1995**, *51*, 3671.
- (35) McElroy, K.; Simmonds, R. W.; Hoffman, J. E.; Lee, D.-H.; Orenstein, J.; Eisaki, H.; Uchida, S.; Davis, J. C. *Nature* **2003**, *422*, 592.